Article

Remote sensing of aerosols at night with the CoSQM sky brightness data

Charles Marseille [2], Martin Aubé [1,2,3,†,*], Africa Barreto [4] and Alexandre Simoneau [2]

[1] Cégep de Sherbrooke, Canada
[2] Département de géomatique appliquée, Université de Sherbrooke, Canada
[3] Physics department, Bishop's University, Canada
[4] Centro de Investigación Atmosférica de Izaña, Agencia Estatal de Meteorología, Spain
* Correspondence: martin.aube@cegepsherbrooke.qc.ca; Tel.: 1-819-564-6350 #4146
† Current address: 475 rue du Cégep, Sherbrooke, Québec, Canada J1E 4K1

Abstract: The aerosol optical depth is an important indicator of aerosol particle properties and associated radiative impacts. AOD determination is therefore very important to achieve relevant climate modeling. Most remote sensing techniques to retrieve aerosol optical depth are applicable to daytime given the high level of light available. The night represents half of the time but in such conditions only a few remote sensing techniques are available. Among these techniques, the most reliable are moon photometers and star photometers. In this paper, we attempt to fill gaps in the aerosol detection performed with the aforementioned techniques using night sky brightness measurements during moonless nights with the novel CoSQM: a portable, low cost and open-source multispectral photometer. In this paper, we present an innovative method for estimating the aerosol optical depth by using an empirical relationship between the zenith night sky brightness measured at night with the CoSQM and the aerosol optical depth retrieved at daytime from the AErosol Robotic NETwork. Such a method is especially suited to light-polluted regions with light pollution sources located within a few kilometers of the observation site. A coherent day-to-night aerosol optical depth and Ångström Exponent evolution in a set of 354 days and nights from August 2019 to February 2021 was verified at the location of Santa Cruz de Tenerife on the island of Tenerife, Spain. The preliminary uncertainty of this technique was evaluated using the variance under stable day-to-night conditions, set at 0.02 for aerosol optical depth and 0.75 for Ångström Exponent. These results indicate the set of CoSQM and the proposed methodology appear to be a promising tool to add new information on the aerosol optical properties at night, which could be of key importance to improve climate predictions.

Keywords: Artificial Light at Night; Aerosol optical depth ; Radiometry ; Multispectral ; Measurement

1. Introduction

The aerosol optical depth (AOD), which characterize the total aerosol optical extinction at a given wavelength, is a key parameter in the monitoring of aerosol optical properties. AOD is sensitive to aerosol microphysical characteristics (in particular to the vertically integrated number density and to the particulate size distribution). The Ångström exponent (AE) of aerosols is related to the particles size distribution. In the case of hygroscopic aerosols like sea salt or sulfate these parameters are in turn sensitive to local relative humidity.

Many techniques have been developed in order to monitor the spatiotemporal variability of the AOD. A well-established method consists of observing direct solar radiation using ground-based sun photometer networks such as the AErosol Robotic NETwork (AERONET) [1]. This method provides relatively good temporal information but very sparse spatial information because that the data are only acquired at about one hundred stations worldwide. But one important limitation is that sun photometers only operate when the sun shines. Moon photometers were designed to mitigate that limitation. A limited number of AERONET sites are equipped with moon photometers. A second

 doi:10.20944/preprints202108.0181.v1

important technique is based on inversion algorithms, which exploit the atmospherically dominant signal present over dark target pixels in remotely sensed satellite images. This technique has been successfully applied over dense dark vegetation (DDV) and ocean pixels using satellite-based sensors such as the Moderate Resolution Imaging Spectro-radiometer (MODIS, [2]). Satellite-based inversion techniques give more comprehensive spatial information but are limited to daily sampling frequencies and are typically inferior in accuracy. Although the two techniques are somewhat complementary, they do not allow AOD acquisition on a continuous basis.

In this paper, we attempt to partly fill gaps in the spatiotemporal AOD datasets using a detection methodology that links together the AERONET AOD measurements and the zenith night sky brightness measurements acquired with the multispectral Colour Sky Quality Meter (CoSQM) photometer. As a first step towards a worldwide CoSQM network, four CoSQM were installed on the island of Tenerife in the Canarian Archipelago (Spain) at locations differing by their proximity to the lighting sources and by their elevation. The first goal for establishing such a network was to characterize the sky brightness over the island. This is of interest because of the presence of important astronomical facilities on Tenerife and La Palma islands. Tenerife is also a master site for atmospheric sensing science thanks to the Agencia Estatal de Meteorología (AEMET) facilities that is a reference in terms of aerosol detection and related instrumental cross calibration capabilities. This paper focuses on Santa Cruz de Tenerife location since light pollution there is intense and the size of the data set is higher than the other locations. This excess of night sky brightness is the fundamental advantage of the proposed AOD retrieval approach. The instrument is periodically maintained since this is the main AEMET office. Further work will show the equivalent results for the other locations.

As a first experiment with the CoSQM data, we present empirical relationships to convert the multispectral Zenith Night Sky Brightness (ZNSB) into multispectral AOD for the site of Santa Cruz de Tenerife. This particular site being the most light-polluted one equipped with a CoSQM on the Tenerife Island.

2. Materials and Methods

2.1. General methodology

The general methodology suggested in this paper to retrieve the AOD out of the CoSQM ZNSB free of moon, twilight, Milky Way and clouds is presented in figure 1. Similar concept to extract AOD out of light polluted skies was initially proposed by Aubé *et al.* [3] in 2005. They suggested the joint use of a night sky radiance model with a high sensitivity spectrometer and adjust the AOD value in the model in order to fit the measured night sky radiance. In this paper, we decided to explore another possibility based on the determination of an empirical relationship between the AERONET AOD and the CoSQM sky brightness. We assume that to be reliable, that method requires a set of data selection filters. We want to exclude the nights contaminated with clouds and exclude all measurement time for which the moon or the sun is below 2 and 18 under the horizon respectively. That elevation angle defines for the Sun the so-called astronomical twilight. On the remaining data, we compare the mean of the first 5 CoSQM data points of any night until midnight to its AERONET AOD equivalent, i.e., the latest values in the interval of 2PM until sunset (last measurements of that day). Such is also done for the morning, where the 5 CoSQM data points are averaged in the interval of 2AM until sunrise and compared to AERONET AOD in the interval of sunrise until 10AM. These values have been obtained empirically based on a visual analysis of the resulting filtered data. The biggest assumption of this method is that during the delay between the AERONET and CoSQM measurements, the AOD is considered to remain stable. If such is the case, once that empirical relationship is found, it is possible to apply the relationship to any CoSQM filtered data. Since that method is empirical, a different relationship could be found for each site. This fact implies that CoSQM should be installed in priority on AERONET sites. Or at least a sun photometer must be installed temporarily close to the CoSQM in order to find the relationship. In this methodology we assume that the only variable affecting the

Preprints (www.preprints.org) | NOT PEER-REVIEWED | Posted: 9 August 2021 doi:10.20944/preprints202108.0181.v1

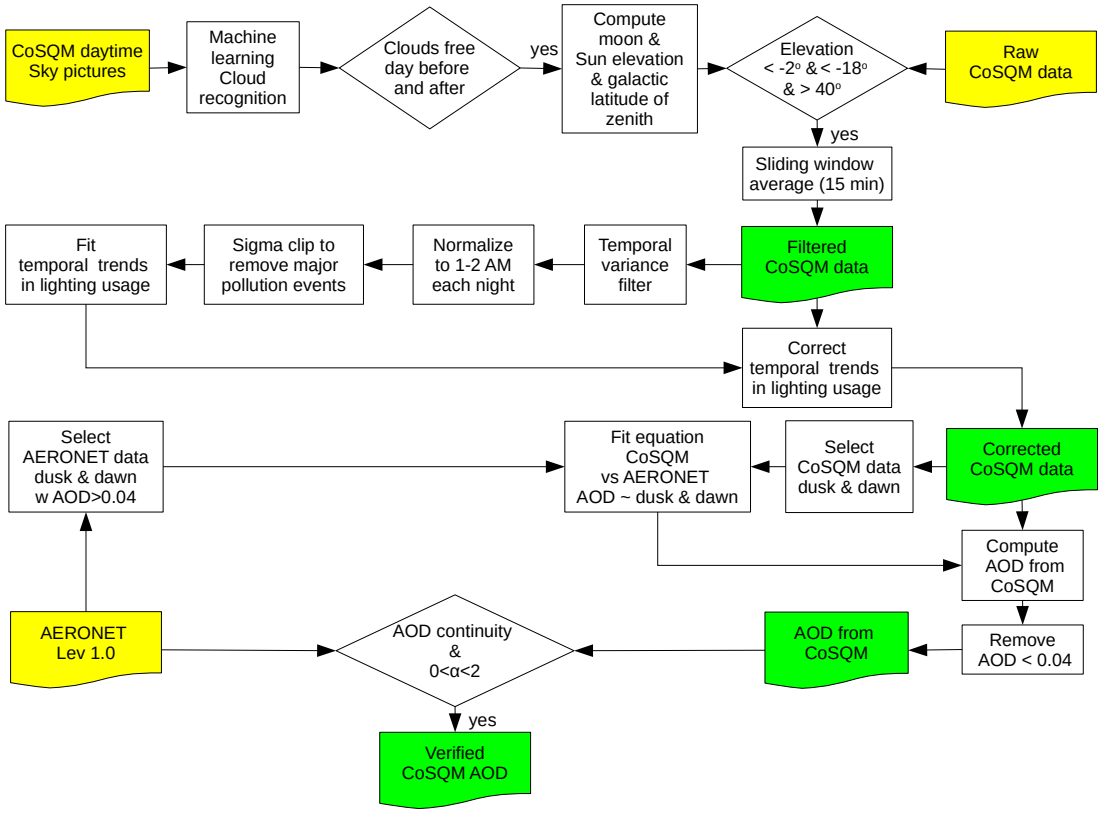

Figure 1. General methodology used to derive the aerosol optical depth out of the CoSQM cloud-free, moon-free and Milky Way-free night sky brightness. Boxes in yellow are input data while green boxes are data produced by the method.

sky brightness is the AOD. It is true that AOD is one of the most important variables to consider [4] but one other important variability is the change in light usage according to the time and date. In this study we assume that that temporal trend is cyclical and then may be inferred and corrected assuming long enough CoSQM time series for the site.

2.2. Instrumentation

2.2.1. The CoSQM system

The CoSQM is a portable device which aims to sample the multispectral properties of nocturnal the artificial light scattered by the atmospheres. It was designed by our group to estimate the spectral properties of the ZNSB. CoSQM is composed of a filter wheel with five different spectral transmittance in the visible range (clear, red, blue, green and yellow (see figure 3)) that is standing on a step motor in front of a Unihedron's Sky Quality Meter (SQM). The SQM is a sensor dedicated to the monitoring of the nocturnal sky brightness. It is panchromatic with a spectral response encompassing the visible domain with some residual sensitivity in the Near Infrared (NIR) [5]. The SQM sensitivity is close to zero at 1000 nm. The SQM sensitivity from 400 nm to 1000 nm is shown by the black continuous line in figure 3. In the CoSQM, we are using the SQM model LE (SQM-LE) which include its own Ethernet interface. We decided to use the SQM in order to be backward compatible with the large amount of SQM data acquired worldwide to date and considering its high sensitivity and resolution of 0.01 Magnitude Per Squared Arc Second (MPSAS). This unit is an inverted logarithmic scale that represents

Preprints (www.preprints.org) | NOT PEER-REVIEWED | Posted: 9 August 2021 doi:10.20944/preprints202108.0181.v1

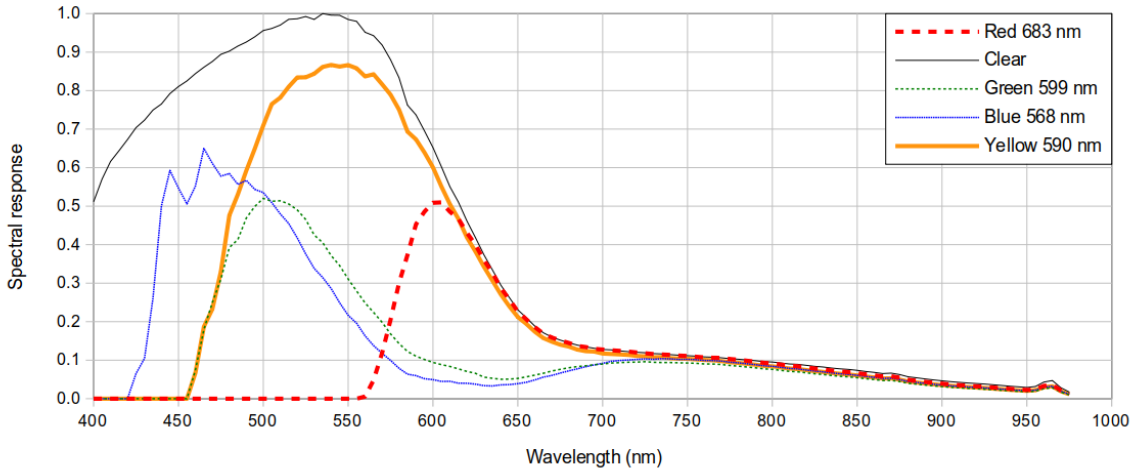

Figure 3. Relative spectral response of the 5 bands of the CoSQM. The thin black line is the spectral response of the SQM-LE as measured by [5]. Other bands are Neewer colour filters in front of the SQM-LE. The nominal wavelength of each band is given in the legend.

the brightness density (per solid angle). Magnitudes were initially developed to characterize the visibility of stars at night. The darker the sky, the higher the MPSAS. The CoSQM device comprises a Raspberry pi (RPI) open source Linux computer. The instrument can be operated remotely via the SSH protocol and the data may be accessed via an integrated web server. The data from all the instruments belonging to our CoSQM network is automatically downloaded every day and stored in a public server. In the second version of the CoSQM, the RPI is configured in a way that the wired network interface is dedicated to the internet connection while the WiFi interface allows the access to the system and data from any mobile device located near the CoSQM. In the version 1, the WiFi interface was not used. Table 1 gives the main properties of the CoSQM v1 and CoSQM v2 devices.

(**a**) (**b**)

Figure 2. The CoSQM device. Panel (a) shows the version 1 of the CoSQM. That specific unit is installed at AEMET Izaña observatory (Spain). Panel (b) shows the second version of the CoSQM. This unit is installed at Saint-Camille (Canada).

The colour detection capability is an important improvement over existing non-imaging detectors. This is particularly important in the context of the drastic undergoing change in the colour of light pollution associated with the transition to the Light-Emitting Diodes (LED) technology. The CoSQM developing philosophy is based on an open science model so that we provide everything under open licence. The methods, drawings, software and documentation can be accessed from Pr. Aubé website [6].

Preprints (www.preprints.org) | NOT PEER-REVIEWED | Posted: 9 August 2021 doi:10.20944/preprints202108.0181.v1

Table 1. Features comparison of CoSQM versions. Optional features and identified with an asterisk.

Feature	v1	v2
Light sensor	SQM-LE	SQM-LE
Filters	Neewer RGBY	Neewer RGBY
Processing unit	Raspberry Pi 3b	Raspberry Pi 4b
Time keeping device	DS3231	DS3231
Sky imaging system	RPI v1.3 (day only)	RPI cam HQ (day & night)
Access to data	Wired ethernet	Wired and WiFi
System state indicator	Red LED	Red LED and WiFi web server
Power source	120 VAC or 240 VAC	5 V - 4 A
Power protection	Nothing	Integrated UPS Hat
Positioning*	GPS	GPS

Table 2. Instruments installed as part of the CoSQM network.

Site name	Version	latitude	longitude	elevation
Saint-Camille (Canada)	2	45 44′ 4.7" N	71 40′ 34.4" W	526 m
Université de Sherbrooke (Canada)	1	45 22′ 25.9" N	71 55′ 22.9" W	372 m
Teide astronomical observatory (Spain)	1	28 18′ 1.6" N	16 30′ 43.9" W	2400 m
Izaña Observatory (Spain)	1	28 18′ 30.8" N	16 29′ 58.6" W	2370 m
Pico Teide (Spain)	1	28 16′ 12.9" N	16 38′ 19.6" W	3550 m
Santa Cruz de Tenerife (Spain)	1	28 28′ 20.8" N	16 14′ 50.4" W	47 m
Universidad Complutense de Madrid (Spain)	1	40 27′ 4.3" N	3 43′ 33.7" W	666 m
Parc Astronomic Montsec (Spain)	1	42 1′ 29.2" N	0 44′ 12.5" E	813 m

2.2.2. CoSQM network

The CoSQM was designed to be used in a permanent installation mode in order to allow the implementation of a worldwide night sky colour detection network. Nevertheless, it is possible to use the CoSQM as a moving device but in such a case a GPS need to be installed. Moreover, one should move slowly because the data acquisition is done every 2.5 min. Since its first release in 2018, 8 CoSQM were installed. These devices are located in a variety of sites concentrated in Canada and Spain. Table 2 gives the list of instruments at the moment of writing. In that table we indicated in bold font the device used in the present paper. Université de Sherbrooke site is peculiar because that there is also a Star photometer installed nearby so that we will ultimately be able to validate the method in comparison to that detection technique.

2.2.3. AERONET sun and moon photometers

The sun-sky-moon multi-band photometer CE318-T [7,8], manufactured by the company Cimel Electronique, is nowadays the only commercial instrument able to perform day and nighttime photometric measurements using the sun and the moon as a light source. The CE318-T is currently the reference instrument in AERONET, together with the old CE318-N standard version [9]. The new photometer version provides additional and enhanced operational functionalities compared with the standard CE318-N [1], mostly related to the improved tracking precision in terms of a new and more sensitive four-quadrant detector in the sensor head and a new control box which uses microstepping technology to improve the pointing resolution. Similarly to the CE318-N, the CE318-T version performs photometric measurements using nine interference filters, with nominal wavelengths centred at 1640, 1020, 937, 870, 675, 500, 440, 380 and 340 nm. Two photodiode detectors allow measurements in the ultraviolet, visible and near infrared spectral range (up to 1020 nm with a silicon detector) and in the near infrared and short-wave infrared (at 1020 nm and 1640 nm with an InGaAs detector). Photometric measurements performed in the ultraviolet are restricted to daytime period, due to the low signal in the UV channels at night. The approximate field of view of the CE318-T is 1.29°.

Preprints (www.preprints.org) | NOT PEER-REVIEWED | Posted: 9 August 2021 doi:10.20944/preprints202108.0181.v1

Once the feasibility of the Cimel CE318-T photometer to retrieve AOD at nighttime from lunar observations was assessed [7,8,10,11] a 'provisional' lunar AOD product was released in the AERONET website. However, AERONET team recognized the presence of anomalies in the data and they don't recommend its use for scientific publications [12].

2.2.4. Meteorological State Agency of Spain (AEMET) facilities

Three of the eight CoSQM that forms the network described in Table 2 were installed in AEMET facilities. This is the case of the stations at Santa Cruz de Tenerife (28.47°N, 16.25°W, 52m a.s.l.), Izaña Observatory (28.31°N, 16.50°W, 2401m a.s.l.) and Pico Teide (28.27°N, 16.64°W, 3552m a.s.l.), located in Tenerife (Canary Islands, Spain), managed by the Izaña Atmospheric Research Centre (IARC) [13]. The subtropical location of this archipelago entails the existence of a strong temperature and moisture inversions in the lower troposphere [14], modulated by quasi-permanent subsidence conditions at this latitude as a result of the descending branch of the Hadley-cell. As Carrillo *et al.* [14] found, one or two sharp temperature inversions or transition layers below the 700 hPa level can be found in the lower troposphere, limiting the humid and well-mixed marine boundary layer (MBL) to the dry and clean free troposphere (CFT) above. The top of the MBL, as an interface between these two very different air masses, is readily visible by the presence of quasi-permanent stratocumulus clouds frequent at this latitude, which have a critical role preventing the arrival of anthropogenic and light pollution from lower altitudes. Another critical feature of Tenerife is the proximity to the African continent, entailing a strong influence of Saharan desert aerosols in the climatology of the three stations. The archipelago is located within the dust transport mainly in summer, as an elevated dust layer (the Saharan Air Layer or SAL) transported above the MBL at subtropical latitudes with a strong impact on the subtropical free troposphere over the North Atlantic [15–17]. Sporadic dust outbreaks can also affect the islands in winter, mostly restricted to lower levels, within the boundary layer [15,18]. These dust events are called "Calima".

Santa Cruz de Tenerife Observatory is an urban station located within the MBL close to the city harbour. As a consequence, the aerosol regime at this station is dominated by coarse mode sea-salt aerosols well mixed with fine mode anthropogenic pollution, formed as a mixture of different anthropogenic sources [19–21]. Mineral dust particles also influence the aerosol climatology at the station, mainly from spring to autumn [20] but also in July–August [21]. As Rodríguez *et al.* [22] have found, the urban scale transport of air pollutants in this station is mainly driven by breeze circulation. Guirado-Fuentes [23] provided a complete aerosol characterization of this site. This author found that the AOD at 500 nm is typically lower than 0.15 and the Ångström Exponent calculated using 440-870 nm spectral bands (AE) is lower than 0.5. These maritime clean conditions are observed 60% of the year.

Izaña and Teide Peak Observatories are two free troposphere stations mainly characterized by clean background conditions, especially at nighttime, when the subsidence flow is reinforced. The predominant pristine conditions at the sites explained the historical importance of Izaña as a reference station for in situ and remote sensing atmospheric measurements, being designated by the WMO as a CIMO test bed for aerosols and water vapour remote-sensing instruments [24]. The two high-mountain stations can be sporadically affected by dust-loaded Saharan air masses mainly in summer, impacting the subtropical free troposphere [15–17]. Guirado-Fuentes [23] performed a detailed aerosol characterization at Izaña, finding that predominant clean background conditions are observed at the station (48% of the year with AOD at 500 nm below 0.05), while dust conditions can be associated to AOD at 500 nm higher than 0.10 and large particles with AE values lower than 0.60. These contrasting atmospheric conditions allow the methodology presented in this paper to be performed under a wide range of AOD values: from pristine to moderate dust loads.

 doi:10.20944/preprints202108.0181.v1

2.3. Filtering CoSQM and AERONET data

To determine the AOD correlation, data points must be filtered for the presence of undesired sky brightness contributions so that the remaining variations are solely attributed to the AOD. In this work, data filtering was applied to the CoSQM instruments only, followed by the comparison with CE318-T Level 1 respecting the same filtering. Also, the filtering time is reduced if one assumes the CE381-T instruments are subject to the same sky conditions as the CoSQM which is the case in this paper. The order in which the different filtering steps are presented is based on the order in which filters are applied in the calculations of the code. The filtering order is optimized to reduce the computing time. Indeed, the cloud filtering sliding window is sensitive to consecutive values and must be done in the first steps before any other filtering is applied (or else filtering artefacts emerge).

2.3.1. Clouds

The presented method uses 3 different successive cloud filtering techniques explained below:

1. **Machine learning cloud recognition**: A multi-step algorithm has been written to determine the presence of clouds in rpi cam pictures taken at intervals of 15 minutes during daytime on each CoSQM. The combination of a residual network (ResNET) and a cyclic generative adversarial network (CycleGAN) generates a binary picture where clouds are detected from the background. Simply put, the RESNET+CycleGAN changes the whole original picture through a deep convoluted network to isolate the elements signatures (clouds, background) while finding the specific pixels where each signature is present. The combination returns a product that is tested with an adversarial network compared to 2 tagged sets of images (clouds/no clouds). The confirmation dataset is easily created with rapid human visualization of a random subset of pictures classified in 2 distinct groups. Following training of the model, all pictures are transformed by the resulting function and a count of the cloud contaminated pixels is made for each picture. Since a picture is taken every 15 minutes, these results inform on cloud density through time. A threshold of cloud density per picture per day is then applied which represents the criterion for the first cloud screening. If 90% of the data pixels are cloud free both the day before and the day after a night of measurements, all data points for this night are conserved, else removed. This percentage has been determined based on a visual analysis of a 30% random subset of the entire Santa Cruz de Tenerife dataset containing 21588 images, where the temporal variance described below was used to evaluate the presence of clouds for these nights. The results of the algorithm convergence after 30,000 epochs are presented in figure 4, where the original pictures are first transformed to binary clouds/no clouds pixels and finally an attempt at cloud removal with the same algorithm. This last step is not used in this project but was an interesting attempt at correcting pictures containing clouds. It also serves as a verification tool since if the end picture appears to be cloud-free by visual analysis, the cloud detection works. The accuracy of this method has been estimated to 85% since the standard machine learning evaluation criteria of precision has not been applied to this specific algorithm. This value has been empirically determined by looking at 100 random results and qualifying each one on a scale of 1 (bad) to 5 (good). Further evaluation work on this approach shall show the best and worse conditions of application.
2. **Temporal variance**: A sliding window filter of empirically selected width is applied after the above filtering is done. Care must be taken at this step to not be too aggressive on the filtering, else the short and intense events of particle loading are also filtered, such as short Calima events. It must be noted that these filtering parameters will strongly depend on the study location. This is discussed later and represents a challenge considering the small number of data points after all filtering steps are applied which, in this specific location, makes a total of 2698 data points per band from a total pre-filtered 100160 data points (2.7%). The selected width for Santa Cruz de Tenerife is a 12.5 minutes interval, representing 5 measurements for each colour band. This value

Preprints (www.preprints.org) | NOT PEER-REVIEWED | Posted: 9 August 2021 doi:10.20944/preprints202108.0181.v1

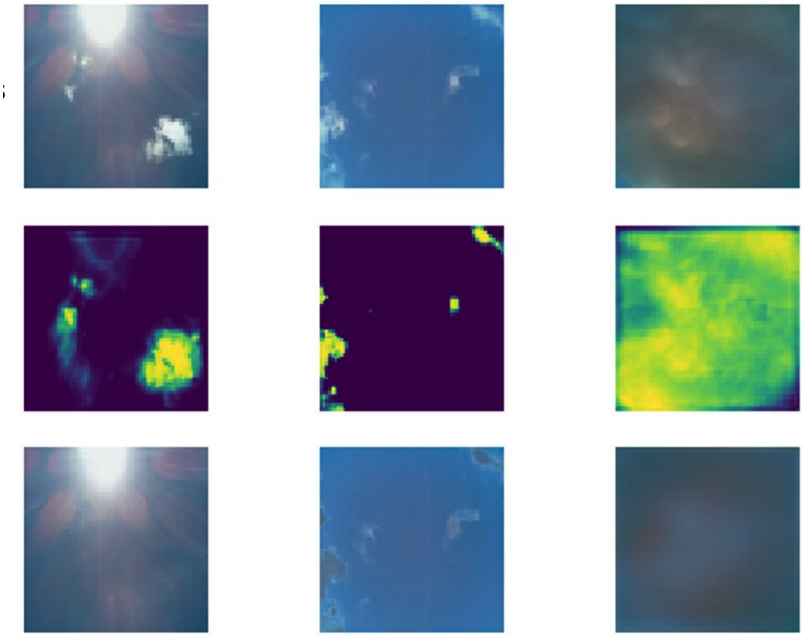

Figure 4. Machine learning algorithm cloud filtering: A combination of a ResNET and a CycleGAN allow converting an RPi cam image (top) to a density map of computed cloud presence (middle), which is used to transform the original image in a cloud-free version (bottom). Images are analyzed the day before and after a night of measurements then CoSQM data is filtered if more than 10% of images contain clouds. Although not used in this project, the corrected product could help obtain cloud corrected ZNSB data with nighttime images if improved and trained with a bigger dataset.

was chosen as it removed the remaining high variance/low MPSAS values while leaving the known Calima events in the dataset, thus adding high AOD values to the correlation function. Since this filtering is applied individually to each night, the first and last measurements of a night are not modified by the nature of the sliding window. This effect was found to be negligible for the correlation results discussed further. A challenge imposed by the instrument is the fact that the 667 nm channel shows a variance twice as large as the other channels. As seen in figure 6, CoSQM measurements higher than 19.95 MPSAS show a large variance which does not pass the temporal variance filter. To fix this problem, the filter only treats the clear band measurements (no filter) which offers a higher signal-to-noise (SNR) ratio. The data points of the other colour bands are then filtered for the same moments the clear channel is filtered. We have confirmed that this high variance in the 667 nm band is also observed for other colour bands when they reach the same 19.95 MPSAS value. This confirms that the variance is not a physical phenomenon specifically observed on the 667 nm band, but an intrinsic SQM sensor limitation.

3. **Visual analysis**: The data points filtered by the temporal variance filter can sometimes leave points that are most probably caused by a quasi-uniform cloud coverage of the entire CoSQM sensor (see figure 4 for example of such a case). These points are in some cases indistinguishable from clear skies measurements, thus a visual inspection of the sky pictures is needed. These points are first located in time in the entire dataset of CoSQM measurements and the specific images of the pi cam of the associated eve and next day are visually examined and discarded if any of the two shows any definitive presence of clouds. A total of 13 nights of measurements were removed following this step, which represents 4% of the resulting nights contained in the dataset at this step.

As described above, cloud filtering steps are first ran with very restrictive parameters to assure the correlated points are as accurate as possible. From there, if the number of data points is not sufficient,

Preprints (www.preprints.org) | NOT PEER-REVIEWED | Posted: 9 August 2021 doi:10.20944/preprints202108.0181.v1

the parameters are loosened to obtain more correlation values.
The filtering applied to the CoSQM also serves as the filtering criteria for the CE381-T data. Indeed, since the AOD measurements are taken during the day, the filtered dates for the CoSQM, primarily based on the presence of clouds, are also the same for the CE318-T. It must then be noted that the level 1 AERONET products are used for the CE318-T data since the filtering is already applied on the CoSQM (where level 1 means no filtering applied). The use of level 1.5 or level 2 (increased filtering) would potentially remove high aerosol loading events, which are primordial to the correlation fit step of the method. The choice of using the level 1 products is valid based on the primary assumption of the project: AOD variations are slow in time and must be the same during dusk and dawn periods for continuity evaluation.
This step of filtering left 42050 of 100160 measurements (42%) of the entire CoSQM dataset in Santa Cruz de Tenerife, which indicates the important presence of clouds at this location and the emphasis on the cloud screening techniques used in low-elevation sites. Measurements in this context mean a 5 value combination, one for each filter band (Clear, 503, 555, 571 and 667 nm).
The next generation of the instrument now incorporates a starlight camera, enabling the cloud detection algorithm to run during SQM measurements. This will allow a greater number of valid data points since the actual ML cloud screening discards entire nights of measurements and not individual measurements.

2.3.2. Milky Way

Following previous filters, the next contribution to be addressed is the presence of the Milky Way in the instrument's field of view. This step comes before the Sun and Moon filtering since it removes more data points, thus reducing the computation time. From an initial analysis of the data, the passage of the Milky Way in the field of view of the instrument can cause a ZNSB reduction of 0.7 MPSAS. By tracking the angle between zenith and the galactic plane (galactic latitude of zenith) using the Skyfield library and limiting its angle from the zenith at a threshold of 40 degrees, this filtering left 7460 of 100160 measurements (7.4%) of the total data set in Santa Cruz. Considering the limited amount of data available to achieve the aimed goal, we decided to reduce this constraint to 30 degrees, leaving 9.5% of the initial data. The impact of this choice is calculated by taking the average of all data passed through every filtering step, resulting in a mean clear-band sky brightness difference of 0.08 MPSAS (7.6%) between the 40 degree case and the 30 degree case. Results were similar for the four colour bands.

2.3.3. Moon

After the sun, the moon presence is the second most important light source to be assessed. Following the same process and using the same python library, data points are removed if the moon's elevation angle is higher than -2 degrees. This value has been determined by visual inspection of several night measurement series for different moon illumination percentages throughout the period of study. This value is optimized to conserve the most data points while having a moon's brightness contribution to ZNSB as small as possible, in this case in the order of 0.01 MPSAS. After this step of filtering, 5453 of 100160 measurements (5.44%) were left of the entire dataset.

2.3.4. Twilight

The scattering and refraction effects of the sun's rays with the atmosphere near sunset and sunrise increase the sky brightness measured by the CoSQM. The filtering of this contribution is assessed by computing the sun's elevation angle and removing all data points where this angle is higher than 18 degrees below the horizon. The Skyfield python library was used to compute these angles [25]. This step of the filtering left 4987 of 100160 measurements (5.0%). This small contribution to filtering is a consequence of the temporal variance filter that removes the rapidly changing ZNSB data points at sunset and sunrise. Initial evaluation indicates that this value can be extended up to -15 degrees

Preprints (www.preprints.org) | NOT PEER-REVIEWED | Posted: 9 August 2021 doi:10.20944/preprints202108.0181.v1

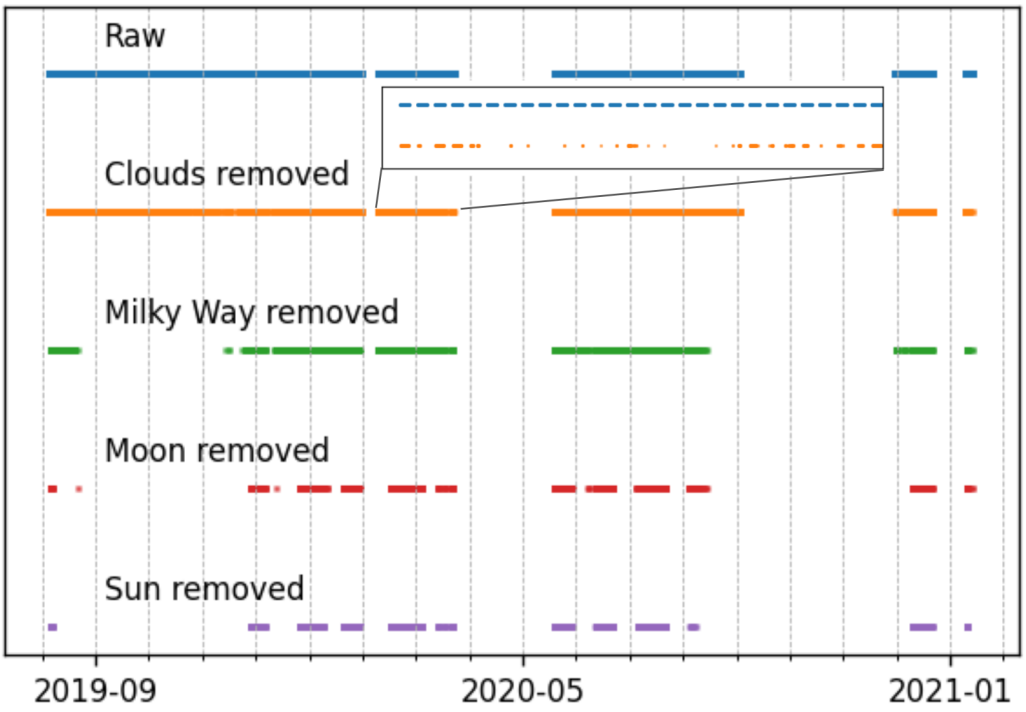

Figure 5. Data reduction through cloud, Milky Way, Moon and Sun filtering. The raw data is successively filtered so the only important ZNSB contribution source left is light pollution emitted by artificial lighting. The size of the markers does not allow to properly see the effect of the cloud screening filtering but a zoom view is provide to outline the reduction following the cloud removal.

Table 3. CoSQM ZNSB sliding window averaging variances

	Clear (no filter)	667 nm	571 nm	503 nm	555 nm
Filtered CoSQM	0.00130	0.0244	0.0048	0.0023	0.001736
Sliding window applied	0.00129	0.0226	0.0027	0.0022	0.001723

for all sites located on Tenerife before an important sky brightness variation is measured. Although, this higher angle only adds 2% of data points. It is not yet confirmed if other sites also show this behaviour. Figure 1 specifies a Sun angle filtering value of -18 degrees for generality purposes, since this is the most restrictive value in astronomy and the one used in this work. Figure 5 shows the data reduction throughout the above defines filters. The initial measurements from the raw data are caused by instrument and/or network failures.

2.3.5. Sliding window averaging per colour band

As mentioned before, the SQM sensor experiences low SNR for high MPSAS measurements. To correct this situation, a second sliding window filter is applied on each band individually for all the dataset. The window duration of 15 minutes (7 measurements) proved to be optimal to reduce the variance while not averaging out the small-scale variations. As seen on figure 6, the measurements above 19.95 MPSAS suddenly show a high variance compared to the lower values. The figure also shows that the filter adequately corrects for high variance in the 667 nm and 571 nm bands, as shown in table 3

Preprints (www.preprints.org) | NOT PEER-REVIEWED | Posted: 9 August 2021 doi:10.20944/preprints202108.0181.v1

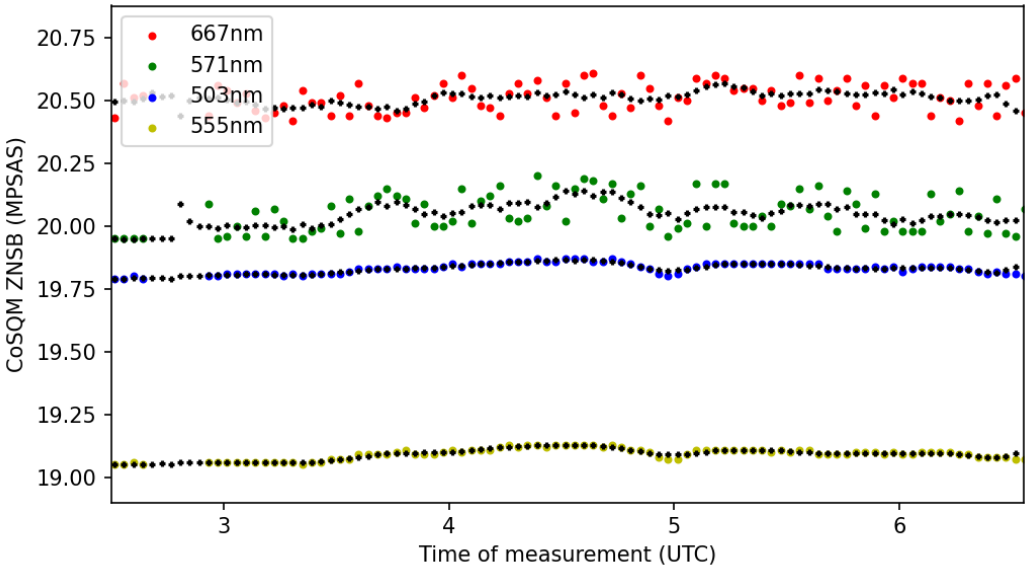

Figure 6. Different variance behaviours of the CoSQM filtered and lighting trend corrected data, showing the important difference between high SNR values (blue and yellow bands) and low SNR (red and green bands) for the night of January 24th, 2020. Preliminary evaluation of the data showed that such variance is also observed in the 571 nm band when the ZNSB goes over 19.95 MPSAS. Black symbols represent the data after applying a 15 min sliding average window over each associated colour band.

2.3.6. Remove recurring temporal trends

Since the ZNSB depends greatly on light pollution sources close to the CoSQM site[26] and that scattered light from light fixtures is the principal source of signal, the temporal trends of lighting usage must be determined to correct for variations of sky brightness associated with human activity or light usage. This information can be extracted directly from the CoSQM filtered data (before the sliding window average step in figure 1). To do so, CoSQM data are evaluated individually for ZNSB as a function of local time of night for each day of week, week and month of year and season. Variations between intervals are evaluated and the longest satisfying interval is chosen to simplify the relationship, while not over fitting the data. Finally, the nighttime dependent contribution to ZNSB is removed from the filtered data. Following this evaluation, we compute a 3rd order correction per band which is applied to the entire data set. The ZNSB is first averaged between 1a.m. and 2a.m. local time for each night. Each night is then normalized with this average and a 3rd-order function is fitted to the result. Finally, the fitted function is subtracted from the ZNSB data as shown on figure 8a for a specific nigh. For these specific data sets, the 1AM to 2AM time interval showed the least variations of ZNSB throughout the nights; hence it was chosen as the reference to normalize the ZNSB trends. This interval may vary between sites, but similar characteristics of the lighting trends would probably be found in near cities since the lighting trends are correlated to population habits and customs and it is reasonable to assume the darkest moment of the night happens in its middle. This interval is also the most probable to give accurate AOD values since it presents the least anthropogenic variations to ZNSB. The figure also shows major differences in the fit parameters for the 667 nm channel compared to the others. This can be caused by a majority of street lighting technologies that present a lower colour temperature such as high pressure sodium and phosphor converted amber LED bulbs (redder technologies). Compared to the private owned lighting, the public portion has a steadier contribution to sky glow since the street lights only turn on once per night. The increase of ZNSB around 4AM can be explained by the private lighting habits of near sources such as bars, restaurants and other nightlife industries that typically close around that time in Tenerife. Finally, the lower end of night reduction of

Preprints (www.preprints.org) | NOT PEER-REVIEWED | Posted: 9 August 2021 doi:10.20944/preprints202108.0181.v1

ZNSB for the 667 nm band seems to indicate an opposite relation compared to the results presented in [27] where cloudless nights ZNSB variations were observed to decrease more in the longer wavelength bands than the smaller. Kyba *et al.* [27] results were obtained in Berlin, Germany.

Figure 9 shows an example of the ZNSB results after all filtering steps for the night of May 23rd, 2020.

2.4. Fitting the AOD vs. sky brightness relationships

Following the filtering steps, only a fraction of the data can be used to derive a relationship between AOD and ZNSB. Indeed, the AOD variation period needed by the proposed technique must be greater than the interval between the last AERONET AOD measurement (typically 8p.m.) and the first CoSQM measurements after filtering steps are applied (typically 10p.m.). This implies that only a subset of the remaining data points are valid correlation candidates, in other words, successive nights and days are necessary to obtain reasonable results. The chosen method consists of the correlation of an average of AOD values around 5 hours before dawn to an average of ZNSB values around 5 hours after dawn (and inversely for dusk). Following the assumption that AOD variations happen on a bigger time scale than this 10 hour interval limit, the ZNSB measured after dawn with the CoSQM should be correlated to the AOD measured before dawn with the CE318-T and inversely for dusk. This approach is intrinsically optimized for steady-state AOD conditions (i.e., where the AOD changes slowly). Dispersion of the points would be caused by rapid fluctuations of AOD happening close to dusk and dawn which is not desirable. These points must be removed since there is no way to confirm the correlation is in fact valid at these moments in time (AOD changes before the first ZNSB measurements are made, reducing the relation's validity).
Since neither instrument has the same multispectral responses, the AE extracted from AERONET products is used to derive the AOD for each CoSQM nominal wavelength following equation 1:

$$\tau_C = \tau_{ref} \left(\frac{\lambda_C}{\lambda_{ref}} \right)^{-\alpha} \tag{1}$$

where τ_C is the AOD at the specific bands CoSQM nominal wavelength, τ_{ref} is the AOD at the specific bands CE318-T central wavelength, λ_C is the specific bands CoSQM nominal wavelength, λ_{ref} is the specific bands CE318-T wavelength and α is the AE from the CE318-T for wavelengths in the 440-870nm range. Since the AE also varies in time, the average of the values is also taken along with the CE318-T AOD measurements and this value is used in the above equation.

Equation 2 was chosen to fit the correlation AOD - ZNSB . This is based on the fact that the magnitude scale is a function of the logarithm of the radiance of the sky which should be reflected through the AOD dependence. Also, AOD falls to 0 at a finite brightness which is assumed to be the ZNSB of the natural sky radiance plus the minimal sky radiance produced by molecules without any aerosols for a given site. Hence, this 0 point will vary between sites that exhibit different lighting conditions. All the most, molecules can also scatter light without aerosol presence which may vary according to the sources of artificial light around the site. It is important to note that the fit function is only valid for a specific interval of ZNSB, which depends on the site for which the fit was obtained. Indeed, the chosen function rapidly decreases towards small AOD values in the range $< 10^{-2}$ for small ZNSB variations in the range 0.1 MPSAS, often allowed by the low SNR high ZNSB measurements in the 667 nm band. Although, the range of sky brightness considered in this approach does not allow such low values to be reached (SB always higher than 17 MPSAS for Santa Cruz de Tenerife in the selected dataset). This then implies that the magnitude scale for each site is bounded in respect to the local light pollution.

$$AOD = -a \times log \left(\frac{ZNSB}{b} \right) \tag{2}$$

Preprints (www.preprints.org) | NOT PEER-REVIEWED | Posted: 9 August 2021 doi:10.20944/preprints202108.0181.v1

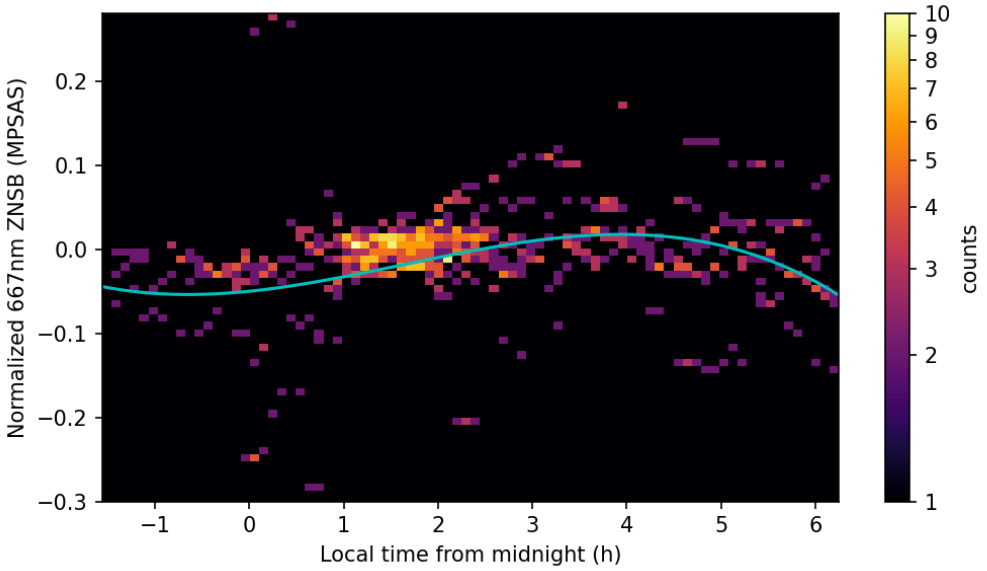

(**a**)

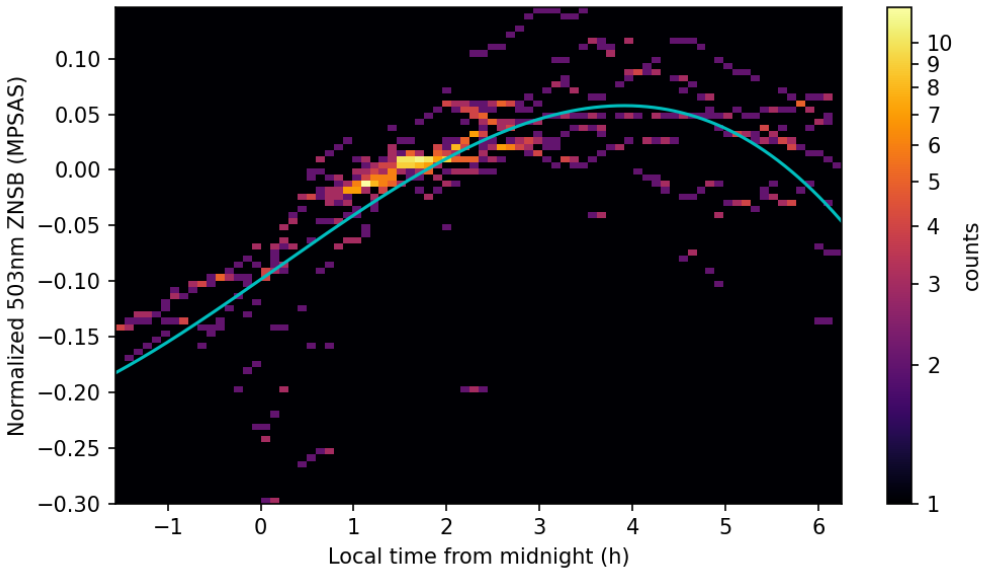

(**b**)

Figure 7. Night trends in lighting habits. Panel (a) shows the correction of normalized ZNSB for the 667 nm band filtered data. Density shows the number of points for each brightness value through the night and the fitted third order night trend. The 3rd order fit was chosen since it adequately follows the lighting trends in urban locations. Panel (b) is the same plot but for the 503 nm band, showing the differences in corrections and evolution of normalized ZNSB throughout the night.

Preprints (www.preprints.org) | NOT PEER-REVIEWED | Posted: 9 August 2021 doi:10.20944/preprints202108.0181.v1

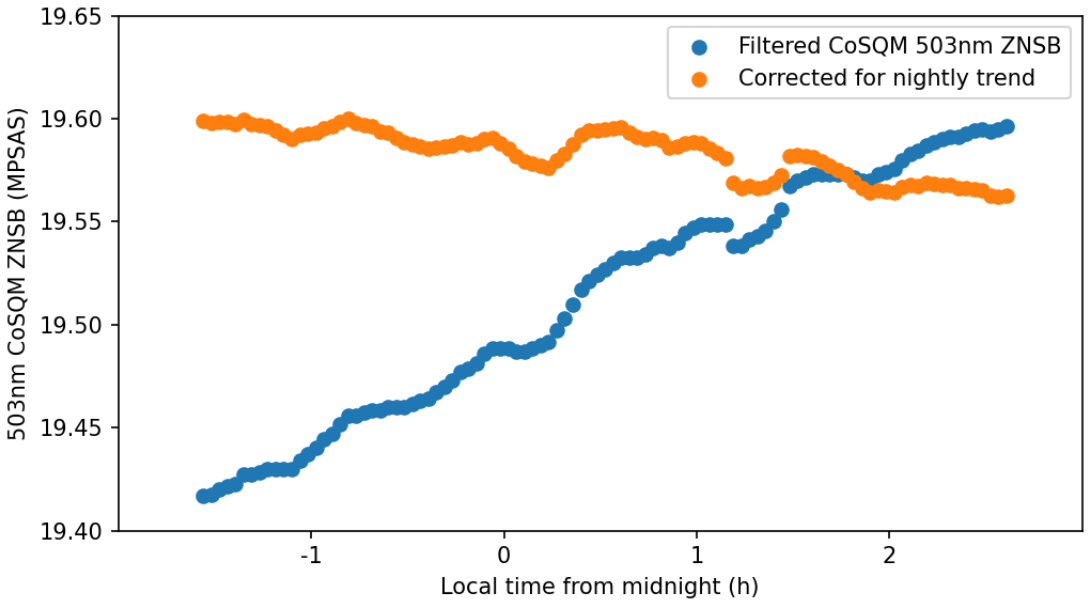

(**a**)

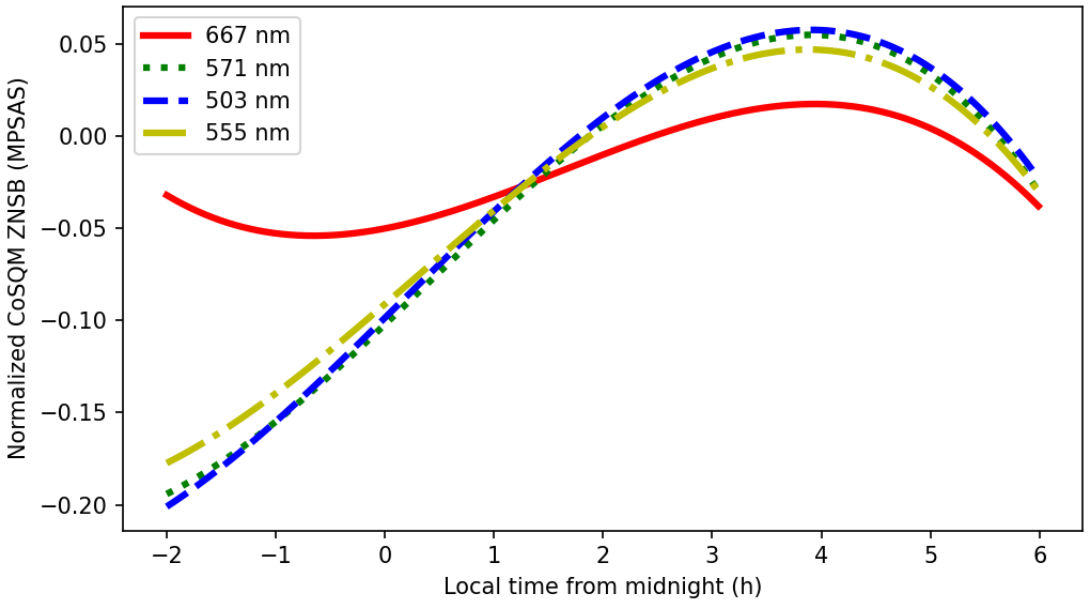

(**b**)

Figure 8. Correction for the light usage trends. Panel (a) is an example of filtered 503 nm CoSQM ZNSB and second order correction of the same data based on the entire band dataset for the night of May 23, 2020. Panel (b) shows a comparison of the correction functions for each CoSQM colour filter band.

Preprints (www.preprints.org) | NOT PEER-REVIEWED | Posted: 9 August 2021 doi:10.20944/preprints202108.0181.v1

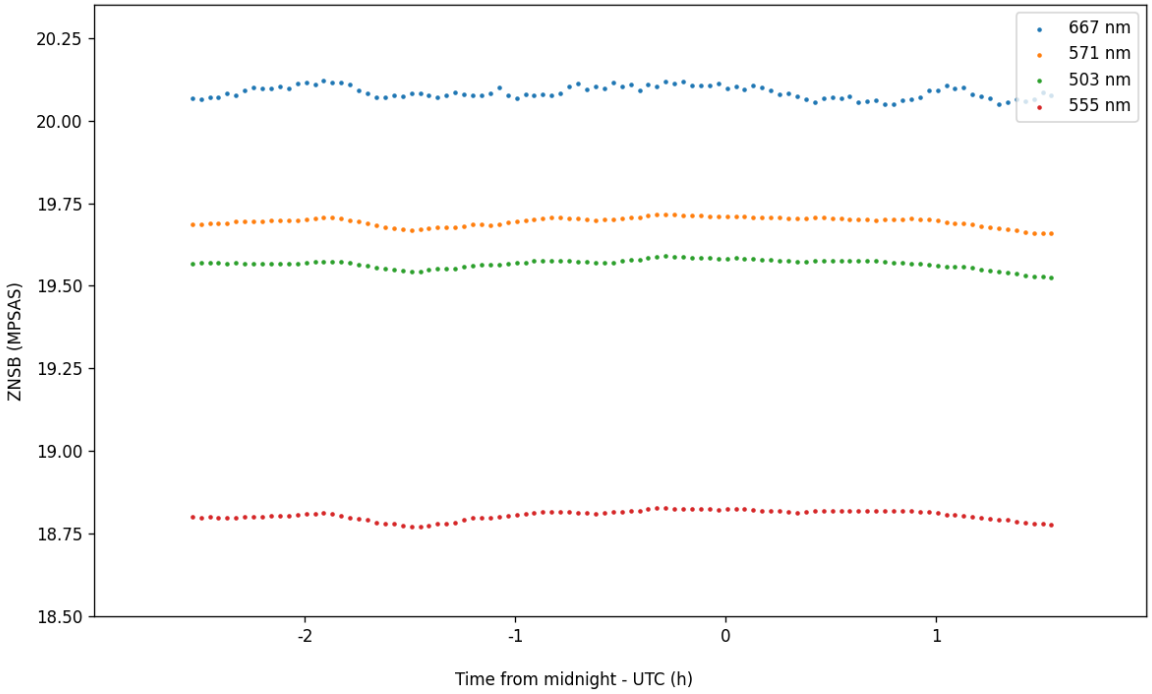

Figure 9. Example night of CoSQM ZNSB filtered and corrected data for the night of May 23rd, 2020. The high variance of data for high MPSAS values is attenuated by the sliding window filter and the nightly trend corrects for ZNSB cyclic nocturnal shifts.

3. Results

3.1. AOD - ZNSB correlations

The correlation results obtained from the above filtering steps are presented on figure 10a for Santa Cruz de Tenerife. Rational functions are fitted to the data using a non-linear least squares method. This choice of function was made based on a non-negative AOD value possibility as well as a decreasing AOD value as a function of sky magnitude. As seen on this figure, a distinction exists between dusk and dawn correlation points which could be explained by the relative humidity variations throughout the night. It is expected that water-soluble or hydrophilic aerosols, especially the marine ones, change their size by absorbing water. This change of size impacts the AOD [28]. This phenomenon is coherent with the relative humidity statistics for dusk and dawn at Santa Cruz de Tenerife. As shown in Figure 10b, relative humidity is generally higher at sunrise which implies larger particle size. This may be linked with increased AOD without change in particle number density. Separate correlation functions have been evaluated but did not result in better AOD-ZNSB and AE continuity so were ignored. We decided to fit a single function per band for the entire dataset. Each band used 51 data points to determine the correlation.

3.2. Daytime vs. nighttime continuity

The time continuity of AOD can be evaluated for the heavily light-polluted case of Santa Cruz de Tenerife with the obtained correlation functions. Considering the uncertain validity of the moon photometer derived AOD nighttime values from AERONET at the time of writing, these products are not presented. Figure 11 shows the results of the continuity for both AOD and AE for the four colour bands of the CoSQM with equivalent AERONET sun photometer AOD in the week of February 20th, 2020 during a Calima event. Figure 12 shows similar results for the week of May 21rd, 2020. The AOD is computed from the ZNSB measurements following the results of figure 10a and equation 2 for

Preprints (www.preprints.org) | NOT PEER-REVIEWED | Posted: 9 August 2021 doi:10.20944/preprints202108.0181.v1

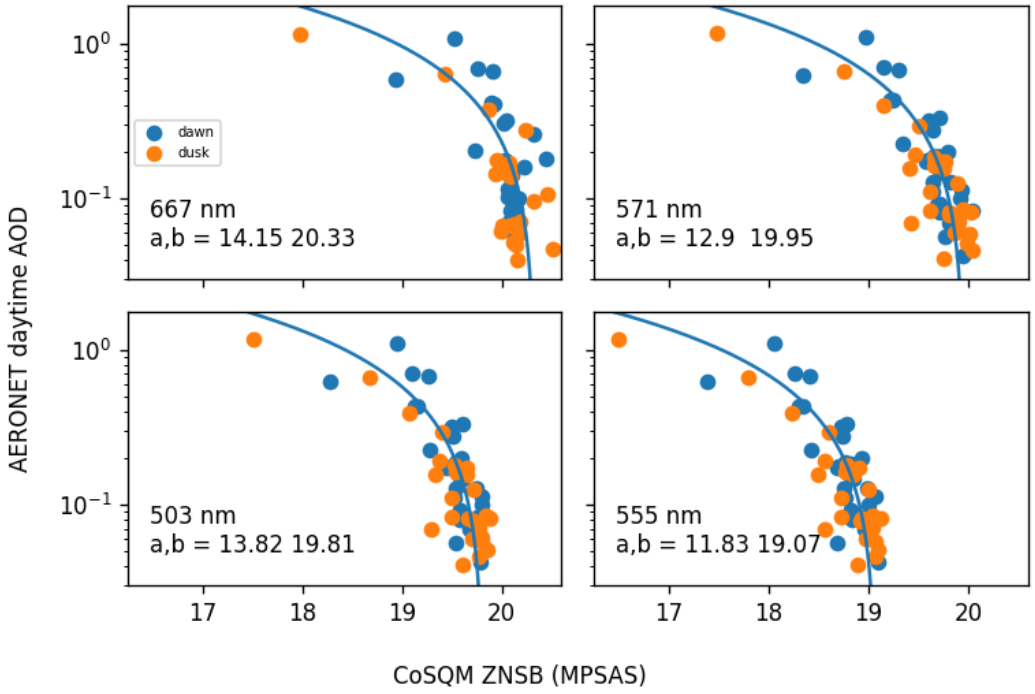

(a)

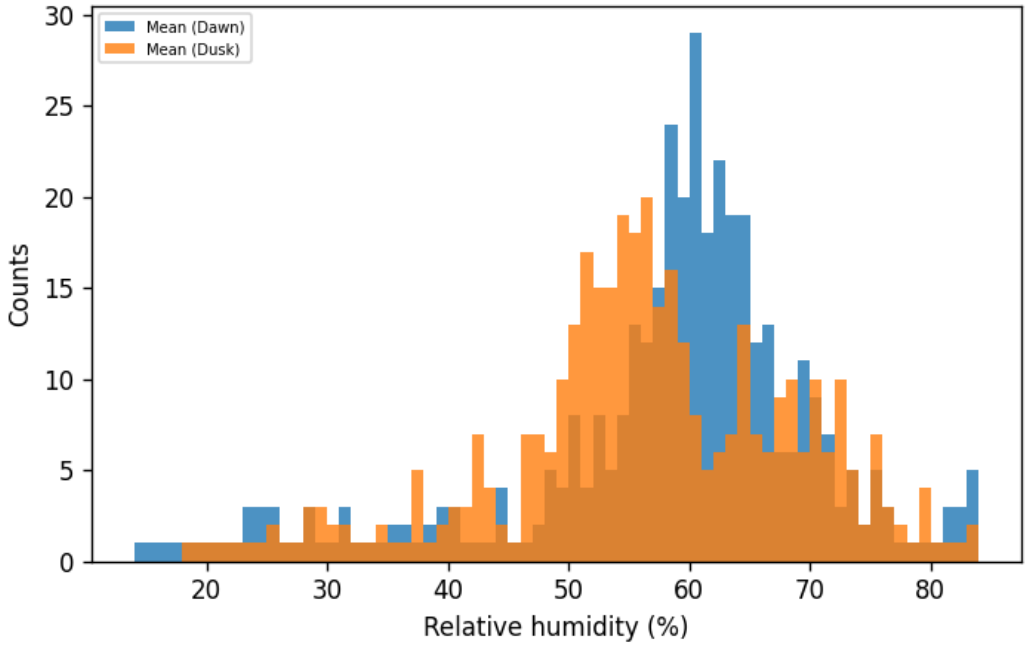

(b)

Figure 10. Relationship between the ZNSB and the daytime AOD. Panel (a) show the fitted function between AOD from CIMEL CE318-T sun photometer and ZNSB from CoSQM multispectral sensor for Santa Cruz de Tenerife location. Dusk and dawn legend specifies the correlated points time interval used for each value. The filtered and averaged data is fitted with equation 2. Parameters a and b correspond to the fitted parameters of equation 2. Panel (b) shows the relative humidity histogram at sunset and sunrise for the year 2020 in Santa Cruz de Tenerife. The higher values associated to sunrise (dawn) explain the difference in the plotted points shown in (a) since higher relative humidity may be associated to higher AOD values.

Preprints (www.preprints.org) | NOT PEER-REVIEWED | Posted: 9 August 2021 doi:10.20944/preprints202108.0181.v1

each band. The AE is then obtained by fitting each set of four AOD computed values (each CoSQM measurement yields one AOD value for each band) with the definition function of the AE:

$$AOD = K\,\lambda^{-\alpha} \tag{3}$$

where K is a coefficient representing the product $\tau_{ref}\ \lambda_{ref}^{\alpha}$ such as is defined in equation 1, λ is the CoSQM nominal wavelength and α the fitted AE. From these products, the AE is filtered following two quality control criteria: (a) Negative values smaller than -0.25 are rejected since negative values do not represent a physical phenomenon and a negative range allows to judge if the AE results are primarily subject to noise or purely invalid. Following the visual analysis of the negative values, the threshold is set to 0 to only keep positive values for the rest of the data processing. (b) A threshold of 2 is imposed based on the common high values observed at this location in the AERONET products throughout the data set period. This serves as a basis for determining which AE values are acceptable from the proposed method. The filtered AE values are finally linked to the measurement dates, themselves used to filter the AOD computed values since non-valid AE values would indicate non-valid AOD values. The results are presented in figures 11a, 11b, 12a, 12b.

Variance throughout the typical night of May 23rd 2020 is shown on figure 13, where the method of the extremes is applied to evaluate the uncertainty of AOD, here 0.02. The selected night is representative of stable state conditions.

The theoretical dependency of ZNSB as a function of distance for multiple AOD values is shown on figure 14a. This plot is from Simoneau *et al.* [4]. It can be seen that in cases where contributing light sources are located either near the observer (<2 km) or far from it (>20 km), good determination of AOD is possible given the high dynamic range of values. Figure 14b then shows the radially integrated contribution maps for AEMET research centre of Santa Cruz de Tenerife. This plot was generated with the Illumina v2 [29,30] model using the light inventory developed by Aubé *et al.* [29]. As can be seen, 90% of the light source's contribution is located in a mean radius of ≈2.5 km and 99% under ≈8 km. This indicates that this site is a good candidate for the proposed method because most of the contribution lighting devices are located in the low interval that presents good discrimination of AOD, as determined from figure 14a.

4. Discussion and conclusion

The exposed method of AOD determination is shown to be possible for the specific site of Santa Cruz de Tenerife since it is a highly light-polluted site and the majority of the contribution of ZNSB from light sources is located inside less than approximately 2.5 km, where AOD dynamic range is high (see figure 14a). This was also made possible since enough data points were remaining after the numerous ZNSB filtering steps, and an apparently realistic correction of the nocturnal lighting trends. The latter is of the upmost importance since it as a direct influence on the AOD values obtained from the method. Indeed, if a wrong correction is applied, the resulting AOD will not correlate with the AERONET product and will give high variance fit values which were shown to cause multiple problems (see AE results of figure 13b). The computed fit functions show high dispersion around small AOD values around $10^{-}1$. This is caused by the filtering parameters which are set to obtain as much valid data points as possible for the correlation and to avoid a filtering bias (for example keeping only summer time data points). A higher number of valid measurements would allow to possibly reduce this dispersion since filtering would be increased and confirm the above assertion. Furthermore, the upcoming version of the instrument will allow short time detection of cloud presence which affects the presented results. This is thought to be the most influential factor of dispersion of the correlation function. The uncertainty of the method for Santa Cruz de Tenerife can be evaluated from figure 13 where the maximum variations are 0.02 for AOD and 0.75 for AE (although more analysis on the latter is needed to conclude this value). This high value for the AE is thought to be caused by the low SNR measurements and because the red band wavelength is close to other bands wavelength which implies

Preprints (www.preprints.org) | NOT PEER-REVIEWED | Posted: 9 August 2021 doi:10.20944/preprints202108.0181.v1

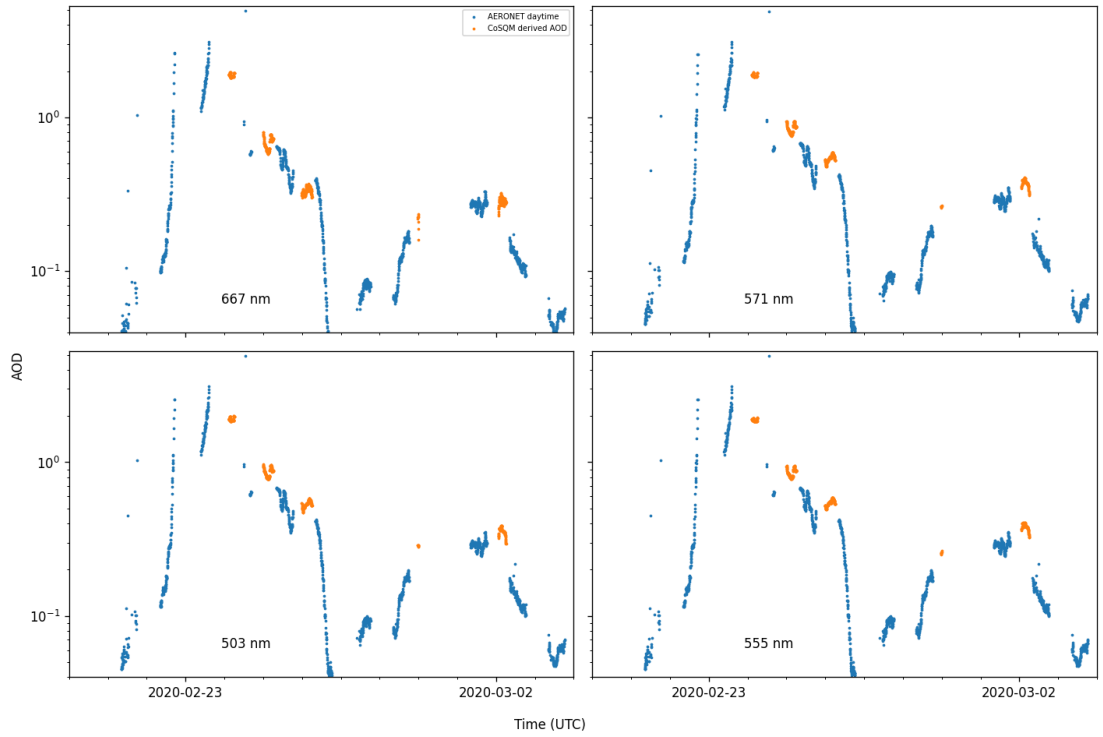

(a)

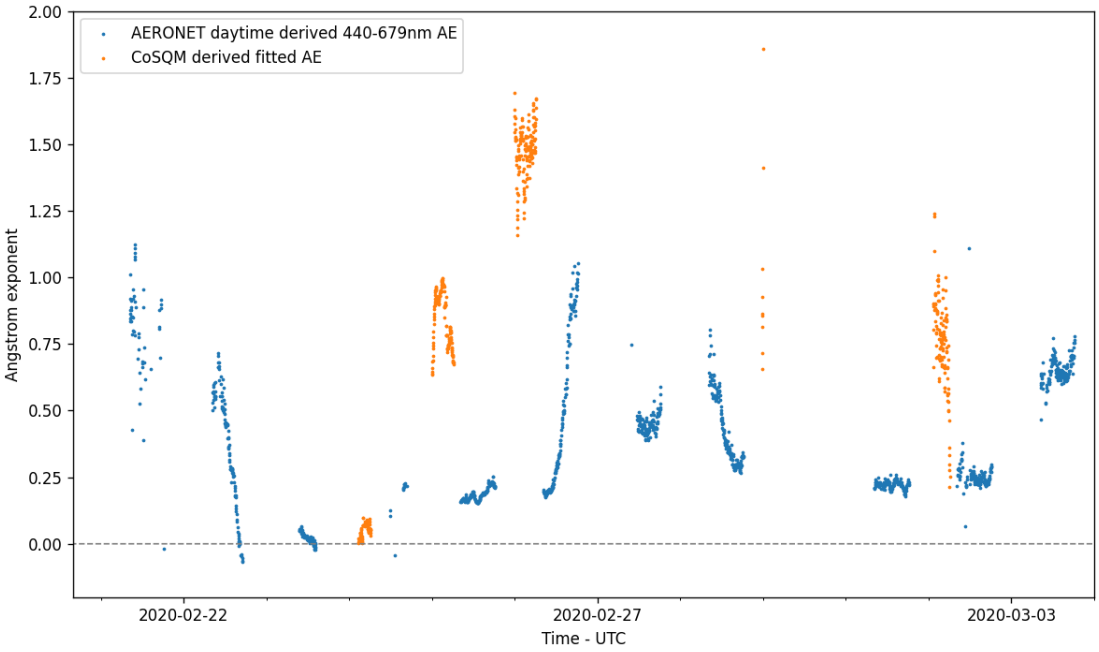

(b)

Figure 11. Continuity of ZNSB derived AOD and AE values compared to AERONET daytime sun photometer measurements during and after a Calima event. Panel (a) shows the AOD for the 4 CoSQM bands and panel (b) the AE derived from a fit of equation 3 on CoSQM AOD values compared to AERONET 440-675 nm daytime sun photometer measurements.

Preprints (www.preprints.org) | NOT PEER-REVIEWED | Posted: 9 August 2021 doi:10.20944/preprints202108.0181.v1

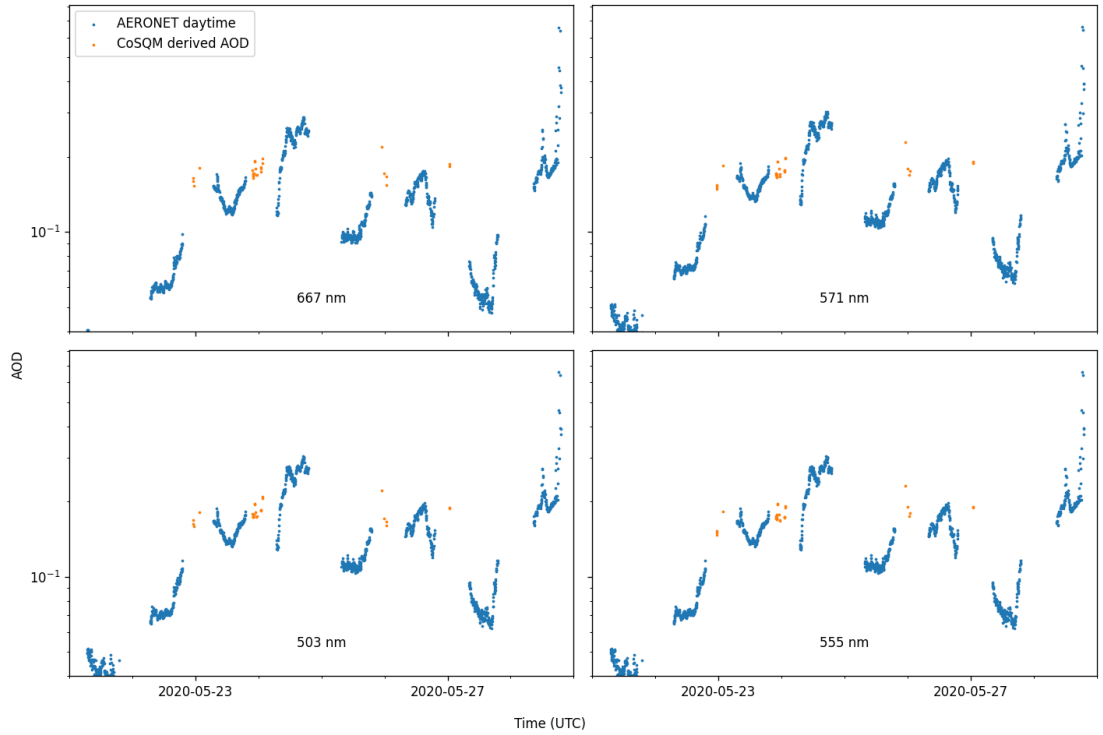

(**a**)

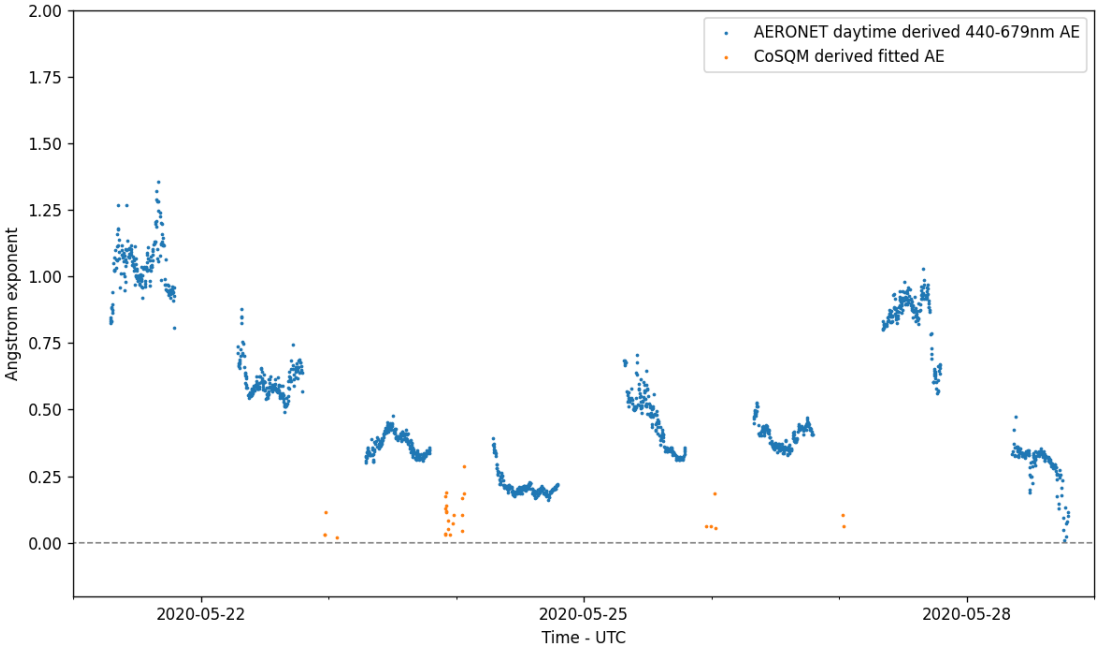

(**b**)

Figure 12. Continuity of ZNSB derived AOD and AE values compared to AERONET daytime sun photometer measurements during typical conditions. Panel (a) shows the AOD for the 4 CoSQM bands and panel (b) the AE derived from a fit of equation 3 on CoSQM AOD values compared to AERONET 440-675 nm daytime sun photometer measurements.

Preprints (www.preprints.org) | NOT PEER-REVIEWED | Posted: 9 August 2021 doi:10.20944/preprints202108.0181.v1

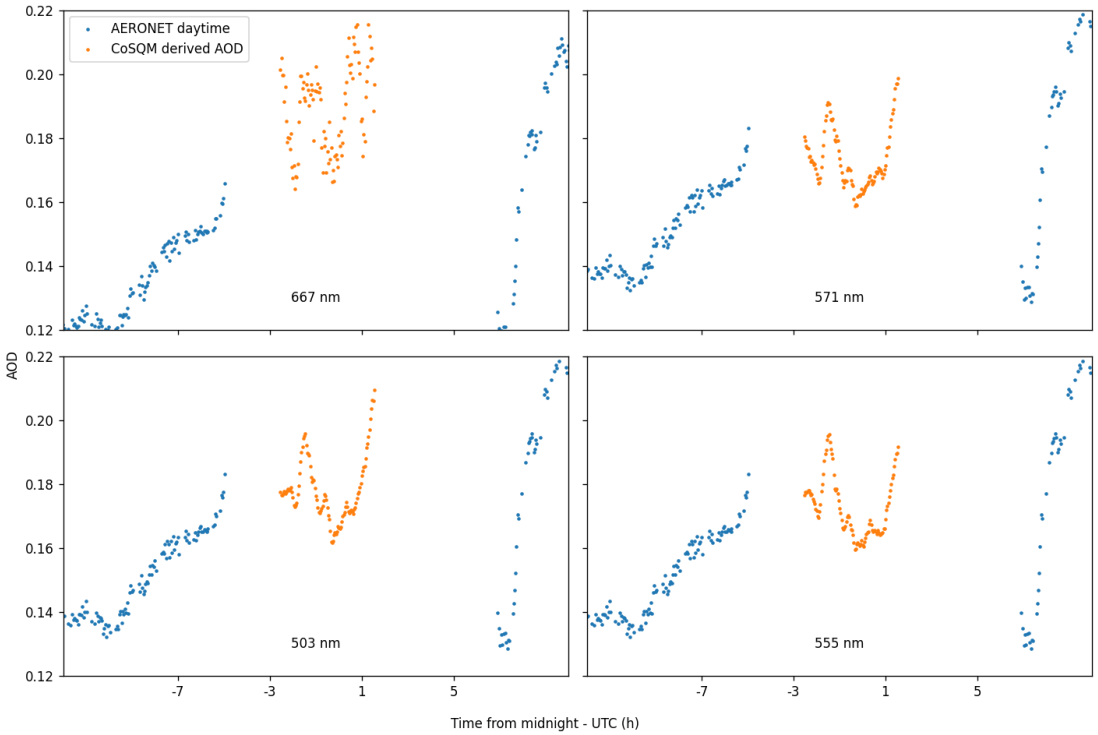

(**a**)

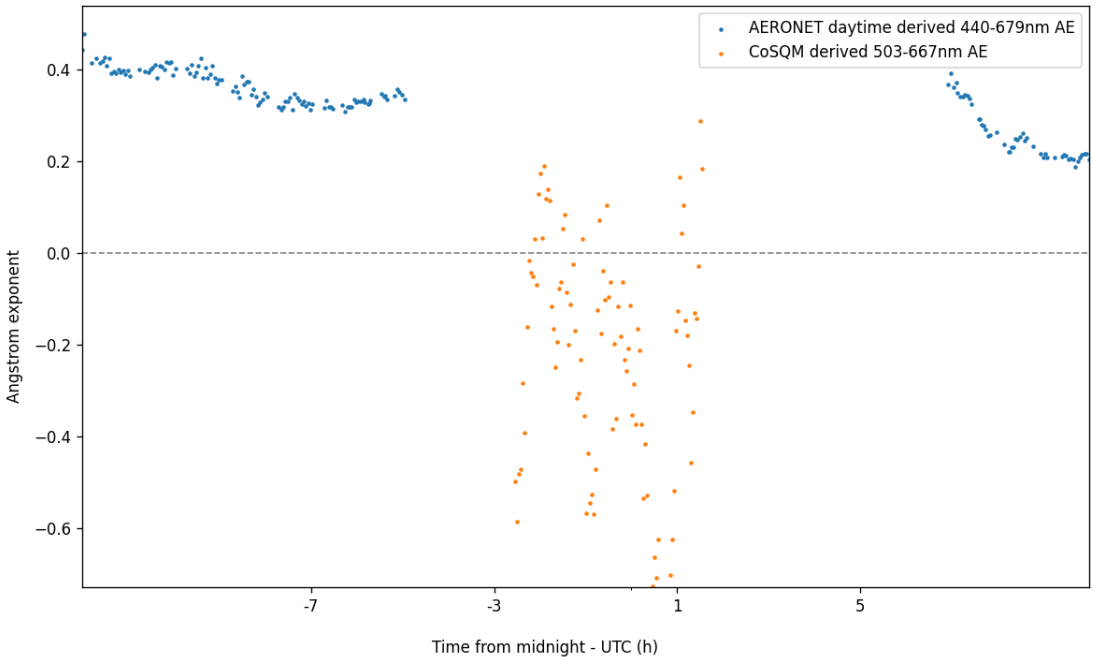

(**b**)

Figure 13. AOD and AE variance for the steady night of May 23rd 2020. On panel (s) an AOD uncertainty of 0.02 can be evaluated if the variations are not considered of physical origin. Panel (b) show the AE for the same night as in (a). The negative values are caused by the high variance of ZNSB values for very dark skies conditions (higher than 19.95 MPSAS).

Preprints (www.preprints.org) | NOT PEER-REVIEWED | Posted: 9 August 2021 doi:10.20944/preprints202108.0181.v1

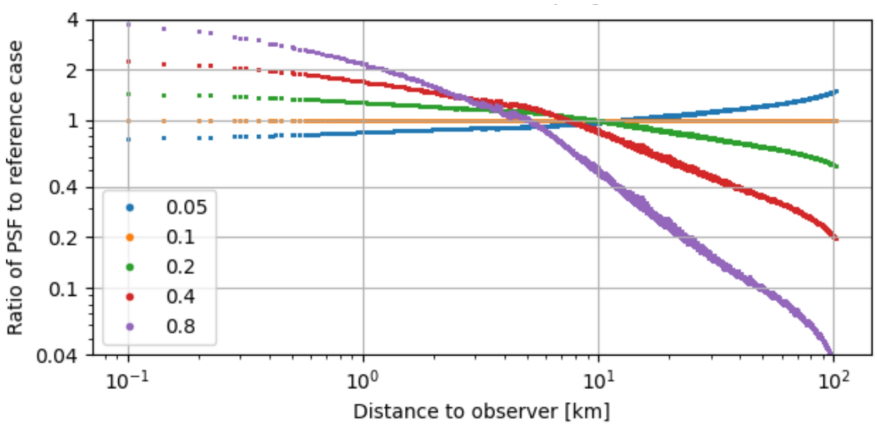

(**a**)

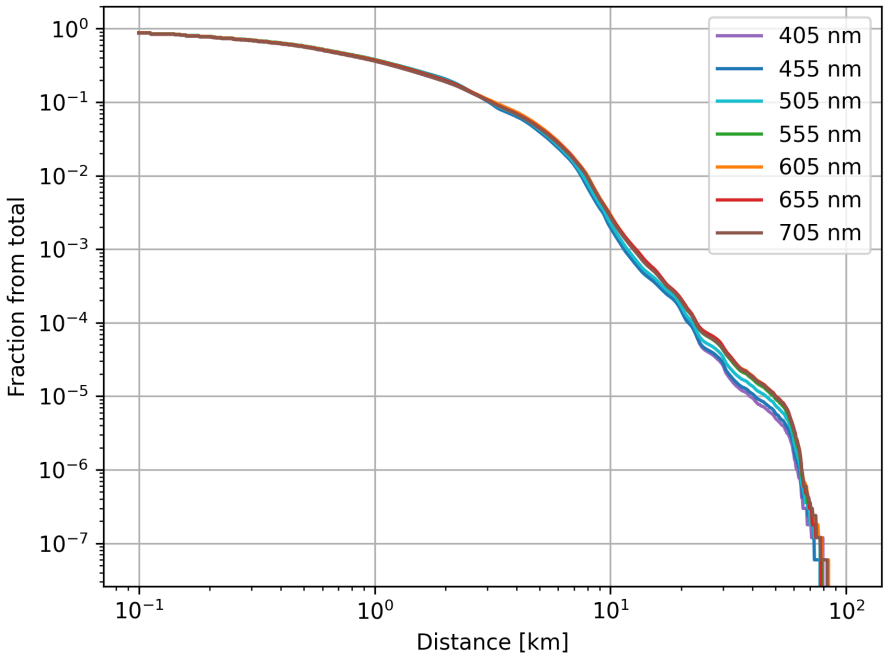

(**b**)

Figure 14. Most important source to the ZNSB-AOD relationship. Panel (a) shows the dependence of relative sky brightness with the distance from sources to observer looking at zenith for different AOD values. The modelled case is for lamps having 5% Upward Light Output Ratio, a wavelength of 550 nm, an AOD of 0.1 and an Ångström exponent of 1.3. These figures come from [4]. The figure indicates that the correlation function should better discriminate various AOD for sites having most of their light source either near the CoSQM (<2 km) or far (>20 km). Panel (b) shows the fraction of the ZNSB coming from within a given radius. The plot is for the AEMET location of Santa Cruz de Tenerife for AOD value of 0.13 and AE of 0.6 (representative of the average value for this site in 2020). Calculations were made with Illumina v2 model [29]. Contributions are shown for each simulated wavelength. 90% of the ZNSB is coming from inside a radius of $\approx$ 2.5 km and 99% from inside a radius of $\approx$ 8 km.

Preprints (www.preprints.org) | NOT PEER-REVIEWED | Posted: 9 August 2021 doi:10.20944/preprints202108.0181.v1

higher uncertainty on the fitted AE parameters. Another factor is that the CoSQM colour bands overlap each other, as seen on figure 3. This implies that the measurements are not independent from each other, increasing even more the offset to AERONET results when AE fits are computed. On the other hand, the high variance of AE makes it possible to discriminate the most valid computed CoSQM AOD values. As of now, our results seem to show considerable variations compared to AERONET but there is no way to conclude that they are erroneous without the use of nighttime AOD products from another instrument. The AOD uncertainty is based on the worst-case scenario since we believe the nocturnal variations to be caused by physical phenomenons, such as relative humidity levels rising as well as human activity decreasing throughout the night. The resolution of the SQM sensor is 0.01 MPSAS, which by the correlation function equates to an AOD of 0.005. This shows that the selected SQM sensor is adequate for the proposed method. Also, some nights show small AOD temporal variations of the order of 0.1 and a steady transition from one day to the other, which seems to indicate that the variations observed are not purely random and that the uncertainty would be lower than previously estimated for nights with low ZNSB (high SNR).

In this paper we presented an innovative method to determine the AOD at night by observing the light pollution scattered by the atmosphere. This new method appears to be promising, especially for heavily light-polluted sites with many nearby light pollution sources located within a few kilometres. Such a method add new information on the optical properties of aerosols and therefore may have a significant impact for improving future global climate model predictions.

The evaluation of the method in the 3 other locations on Tenerife Island (see table 2) will be presented in a future work. It is not trivial if the method will work well for these sites because an important part of the light for at least Izana and Observatorio del Teide seems to come from sources concentrated around a distance of 10 km which is the critical zone with almost no possibility to discriminate AODs as shown in figure 14a. Actually, these sites do not have significant sources of light pollution inside a radius of a few kilometres. Such situation may mitigate the possibility to distinguish different values of AOD. The case of Pico Teide may be different because in that case many contributing sources must be further than ≈13 km where the dynamic range for discriminating AOD is high (see figure 14a). On the counterpart, we expect the signal-to-noise to be lower given that the site is distant from sources and therefore lowly light polluted. Future work will also aim to compare AOD results obtained from star photometry to the technique described in this paper. The advantages of this approach rely on the low uncertainty of the star photometer measurements (0.01 AOD with the 2 star method [31]) and the same clear sky conditions for simultaneous data point comparison. This would allow an absolute calibration and the uncertainty of the exposed method could be better determined. At the time of writing, a remote-controlled star photometer and a mini-MPL lidar are being installed at the Sherbrooke site listed on Table 2 for the above evaluation. In combination with the CIMEL318-T also installed in Sherbrooke, the evaluation of the method in this location looks promising. Also, a new product from AERONET based on the RIMO (ROLO Implementation for Moon's Observation) correction factor (RCF)[32] method giving precise AOD values from moon photometry will be compared to our results. This addition to the continuity evaluation of AOD throughout the years and sites would represent a better basis for correlation since the time interval between an RCF measurement and a CoSQM measurement would be greatly reduced. Finally, the replacement of the actual units with CoSQM V2 will allow nighttime sky pictures to be taken for each measurement sequence (ultimately 2.5 minutes interval) which will greatly increase the total filtered data points (compared to a cloud-free filtering frequency of about 36 hours, or two consecutive days), increasing the accuracy of the method.

Author Contributions: We applied the sequence-determines-credit approach [33] for the sequence of authors which is in order of decreasing contributions. Conceptualization, M.A. ; methodology, C.M. and M.A. ; software, M.A., C.M., A.S.; validation, M.A., C.M.; formal analysis, M.A., C.M.; investigation, M.A., C.M., A.B.; resources, M.A., A.B.; data curation, C.M., M.A., A.S.; writing–original draft preparation, M.A., A.B. and C.M.; writing–review and editing, M.A., C.M., A.B., A.S.; visualization, C.M., M.A., A.S.; supervision, M.A.; project administration, M.A.; funding acquisition, M.A.

Funding: M. A., C. M. and A.S. thanks the Fonds de recherche du Québec – Nature et technologies (FRQNT) for financial support through the Research program for college researchers.

Acknowledgments: We want to thank Ramon Ramos and Antonio Cruz Martin from AEMET office and Miquel Serra Ricart from Instituto de Astrofisica de Canarias who helped with the installation of the CoSQM units on the Tenerife Island. We also thank Professor Normand T. O'Neill for his educated advice concerning this work, and Élysé Lapalme for his help on the cloud screening evaluation. This work has been developed within the framework of the activities of the World Meteorological Organization (WMO) Commission for Instruments and Methods of Observations (CIMO) Izaña Testbed for Aerosols and Water Vapour Remote Sensing Instruments. The authors thank the Aerosol Robotic Network (AERONET) for the aerosol data. AERONET sun photometer at Santa Cruz has been calibrated within the AERONET Europe TNA, supported by the European Community Research Infrastructure Action under the FP7 ACTRIS grant, agreement No. 262,254.

Conflicts of Interest: The authors declare no conflict of interest.

Abbreviations

The following abbreviations are used in this manuscript:

AE	Ångström Exponent
AEMET	Agencia Estatal de Meteorología
AERONET	AErosol Robotic NETwork
AOD	Aerosol optical depth
CoSQM	Colour Sky Quality Meter
FRQNT	Fonds de recherche du Québec – Nature et technologies
GPS	Global Positioning System
LED	Light Emitting Diode
MPSAS	Magnitude Per Square Arc Second
nm	nanometer
RIMO	ROLO Implementation for Moon's Observation
SNR	Signal-to-Noise
SQM	Sky Quality Meter
UPS	Uninterruptible Power Supply
ZNSB	Zenithal night sky brightness

References

1. Holben, B.N.; Eck, T.; Slutsker, I.; Tanre, D.; Buis, J.; Setzer, A.; Vermote, E.; Reagan, J.; Kaufman, Y.; Nakajima, T.; others. AERONET—A federated instrument network and data archive for aerosol characterization. *Remote sensing of environment* **1998**, *66*, 1–16.
2. Kaufman, Y.J.; Tanré, D. Algorithm for remote sensing of tropospheric aerosol from MODIS. *NASA MODIS Algorithm Theoretical Basis Document, Goddard Space Flight Center* **1998**, *85*, 3–68.
3. Aubé, M.; Franchomme-Fossé, L.; Robert-Staehler, P.; Houle, V. Light pollution modelling and detection in a heterogeneous environment: toward a night-time aerosol optical depth retreival method. Atmospheric and environmental remote sensing data processing and utilization: numerical atmospheric prediction and environmental monitoring. International Society for Optics and Photonics, 2005, Vol. 5890, p. 589012.
4. Simoneau, A.; Aubé, M.; Leblanc, J.; Boucher, R.; Roby, J.; Lacharité, F. Point spread functions for mapping artificial night sky luminance over large territories. *Monthly Notices of the Royal Astronomical Society* **2021**, *504*, 951–963.
5. Sánchez de Miguel, A.; Aubé, M.; Zamorano, J.; Kocifaj, M.; Roby, J.; Tapia, C. Sky Quality Meter measurements in a colour-changing world. *Monthly Notices of the Royal Astronomical Society* **2017**, *467*, 2966–2979.
6. Aubé, Martin. CoSQM webpage., 2021. https://lx02.cegepsherbrooke.qc.ca/~aubema/index.php/Prof/CoSQMEn.
7. Barreto, A.; Cuevas, E.; Damiri, B.; Guirado, C.; Berkoff, T.; Berjón, A.J.; Hernández, Y.; Almansa, F.; Gil, M. A new method for nocturnal aerosol measurements with a lunar photometer prototype. *Atmospheric Measurement Techniques* **2013**, *6*, 585–598. doi:10.5194/amt-6-585-2013.

8. Barreto, A.; Cuevas, E.; Granados-Muñoz, M.J.; Alados-Arboledas, L.; Romero, P.M.; Gröbner, J.; Kouremeti, N.; Almansa, A.F.; Stone, T.; Toledano, C.; Román, R.; Sorokin, M.; Holben, B.; Canini, M.; Yela, M. The new sun-sky-lunar Cimel CE318-T multiband photometer – a comprehensive performance evaluation. *Atmospheric Measurement Techniques* **2016**, *9*, 631–654. doi:10.5194/amt-9-631-2016.
9. Giles, D.M.; Sinyuk, A.; Sorokin, M.G.; Schafer, J.S.; Smirnov, A.; Slutsker, I.; Eck, T.F.; Holben, B.N.; Lewis, J.R.; Campbell, J.R.; Welton, E.J.; Korkin, S.V.; Lyapustin, A.I. Advancements in the Aerosol Robotic Network (AERONET) Version 3 database – automated near-real-time quality control algorithm with improved cloud screening for Sun photometer aerosol optical depth (AOD) measurements. *Atmospheric Measurement Techniques* **2019**, *12*, 169–209. doi:10.5194/amt-12-169-2019.
10. Berkoff, T.A.; Sorokin, M.; Stone, T.; Eck, T.F.; Hoff, R.; Welton, E.; Holben, B. Nocturnal aerosol optical depth measurements with a small-aperture automated photometer using the moon as a light source. *Journal of Atmospheric and Oceanic Technology* **2011**, *28*, 1297–1306.
11. Li, Z.; Li, K.; Li, D.; Yang, J.; Xu, H.; Goloub, P.; Victori, S. Simple transfer calibration method for a Cimel Sun–Moon photometer: calculating lunar calibration coefficients from Sun calibration constants. *Appl. Opt.* **2016**, *55*, 7624–7630. doi:10.1364/AO.55.007624.
12. AERONET TECHNICAL DOCUMENT. Lunar Aerosol Optical Depth Computation, 2019. https://aeronet.gsfc.nasa.gov/new_web/Documents/Lunar_Algorithm_Draft_2019.pdf.
13. IARC. IARC webpage., 2021. http://izana.aemet.es.
14. Carrillo, J.; Guerra, J.C.; Cuevas, E.and Barrancos, J. Characterization of the Marine Boundary Layer and the Trade-Wind Inversion over the Sub-tropical North Atlantic. *Boundary-Layer Meteorology* **2016**, *158*, 311–330. doi:10.1007/s10546-015-0081-1.
15. Rodríguez, S.; Alastuey, A.; Alonso-Pérez, S.; Querol, X.; Cuevas, E.; Abreu-Afonso, J.; Viana, M.; Pérez, N.; Pandolfi, M.; de la Rosa, J. Transport of desert dust mixed with North African industrial pollutants in the subtropical Saharan Air Layer. *Atmospheric Chemistry and Physics* **2011**, *11*, 6663–6685. doi:10.5194/acp-11-6663-2011.
16. Rodríguez, S.; Cuevas, E.; Prospero, J.M.; Alastuey, A.; Querol, X.; López-Solano, J.; García, M.I.; Alonso-Pérez, S. Modulation of Saharan dust export by the North African dipole. *Atmospheric Chemistry and Physics* **2015**, *15*, 7471–7486. doi:10.5194/acp-15-7471-2015.
17. Cuevas, E.; Romero-Campos, P.M.; Kouremeti, N.; Kazadzis, S.; Räisänen, P.; García, R.D.; Barreto, A.; Guirado-Fuentes, C.; Ramos, R.; Toledano, C.; Almansa, F.; Gröbner, J. Aerosol optical depth comparison between GAW-PFR and AERONET-Cimel radiometers from long-term (2005–2015) 1 min synchronous measurements. *Atmospheric Measurement Techniques* **2019**, *12*, 4309–4337. doi:10.5194/amt-12-4309-2019.
18. Cuevas, E.; Camino, C.; Benedetti, A.; Basart, S.; Terradellas, E.; Baldasano, J.M.; Morcrette, J.J.; Marticorena, B.; Goloub, P.; Mortier, A.; Berjón, A.; Hernández, Y.; Gil-Ojeda, M.; Schulz, M. The MACC-II 2007-2008 reanalysis: atmospheric dust evaluation and characterization over northern Africa and the Middle East. *Atmospheric Chemistry and Physics* **2015**, *15*, 3991–4024. doi:10.5194/acp-15-3991-2015.
19. González, Y.; Rodríguez, S.; Guerra García, J.C.; Trujillo, J.L.; García, R. Ultrafine particles pollution in urban coastal air due to ship emissions. *Atmospheric Environment* **2011**, *45*, 4907 – 4914. doi:10.1016/j.atmosenv.2011.06.002.
20. Basart, S.; Pérez, C.; Cuevas, E.; Baldasano, J.M.; Gobbi, G.P. Aerosol characterization in Northern Africa, Northeastern Atlantic, Mediterranean Basin and Middle East from direct-sun AERONET observations. *Atmospheric Chemistry and Physics* **2009**, *9*, 8265–8282. doi:10.5194/acp-9-8265-2009.
21. Milford, C.; Cuevas, E.; Marrero, C.L.; Bustos, J.; Gallo, V.; Rodríguez, S.; Romero-Campos, P.M.; Torres, C. Impacts of Desert Dust Outbreaks on Air Quality in Urban Areas. *Atmosphere* **2020**, *11*. doi:10.3390/atmos11010023.
22. Rodríguez, S.; Cuevas, E.; González, Y.; Ramos, R.; Romero, P.M.; Pérez, N.; Querol, X.; Alastuey, A. Influence of sea breeze circulation and road traffic emissions on the relationship between particle number, black carbon, PM1, PM2.5 and PM2.5–10 concentrations in a coastal city. *Atmospheric Environment* **2008**, *42*, 6523 – 6534. doi:10.1016/j.atmosenv.2008.04.022.
23. Guirado-Fuentes, C. Caracterización de las propiedades de los aerosoles en columna en la región subtropical. Ph.D. Thesis, Universidad de Valladolid, 2015. doi:10.35376/10324/13220.
24. WMO. *Commission for Instruments and Methods of Observation,Sixteenth session WMO no.1138*; Saint Petersburg,Secretariat of the World Meteorological Organization, 2014.

25. Rhodes, B. Skyfield: High precision research-grade positions for planets and Earth satellites generator, 2019, [1907.024].
26. Simoneau, A.; Aubé, M.; Bertolo, A. Multispectral analysis of the night sky brightness and its origin for the Asiago Observatory, Italy. *Monthly Notices of the Royal Astronomical Society* **2019**, *491*, 4398–4405. doi:10.1093/mnras/stz3406.
27. Kyba, C.C.M.; Ruhtz, T.; Fischer, J.; Hölker, F. Red is the new black: how the colour of urban skyglow varies with cloud cover. *Monthly Notices of the Royal Astronomical Society* **2012**, *425*, 701–708, [https://onlinelibrary.wiley.com/doi/pdf/10.1111/j.1365-2966.2012.21559.x]. doi:https://doi.org/10.1111/j.1365-2966.2012.21559.x.
28. Yoon, S.C.; Kim, J. Influences of relative humidity on aerosol optical properties and aerosol radiative forcing during ACE-Asia. *Atmospheric Environment* **2006**, *40*, 4328–4338.
29. Aubé, M.; Simoneau, A.; Muñoz-Tuñón, C.; Díaz-Castro, J.; Serra-Ricart, M. Restoring the night sky darkness at Observatorio del Teide: First application of the model Illumina version 2. *Monthly Notices of the Royal Astronomical Society* **2020**, *497*, 2501–2516.
30. Aubé, M.; Simoneau, A. New features to the night sky radiance model illumina: Hyperspectral support, improved obstacles and cloud reflection. *Journal of Quantitative Spectroscopy and Radiative Transfer* **2018**, *211*, 25–34. doi:https://doi.org/10.1016/j.jqsrt.2018.02.033.
31. Ivănescu, L.; Baibakov, K.; O'Neill, N.T.; Blanchet, J.P.; Schulz, K.H. Accuracy in starphotometry. *Atmospheric Measurement Techniques Discussions* **2021**, *2021*, 1–58. doi:10.5194/amt-2021-88.
32. Román, R.; González, R.; Toledano, C.; Barreto, A.; Pérez-Ramírez, D.; Benavent-Oltra, J.A.; Olmo, F.J.; Cachorro, V.E.; Alados-Arboledas, L.; de Frutos, A.M. Correction of a lunar-irradiance model for aerosol optical depth retrieval and comparison with a star photometer. *Atmospheric Measurement Techniques* **2020**, *13*, 6293–6310. doi:10.5194/amt-13-6293-2020.
33. Tscharntke, T.; Hochberg, M.E.; Rand, T.A.; Resh, V.H.; Krauss, J. Author sequence and credit for contributions in multiauthored publications. *PLoS biology* **2007**, *5*, e18.